icrrd
Quality Index Research Journal
INTERNATIONAL CENTER FOR RESEARCH AND RESOURCES DEVELOPMENT article
ISSN Number: 2773-5958, SSM Number: (1347468-T), doi.org/10.53272/icrrd, www.icrrd.com

Removal of Remazol Red RR from Aqueous Solution by Glass Supported Films of Synthesized ZnO Nanoparticles

Mohammad Akter Hossain[1,2]*, Md. Nazmul Kayes[3], Md. Mufazzal Hossain[1]

[1]*Department of Chemistry, University of Dhaka, Dhaka 1000, Bangladesh.*
[2]*Department of Chemistry and Biochemistry, Kent State University, OH 44240, USA*
[3]*Department of Chemistry, University of Barishal, Barishal 8200, Bangladesh*
*Corresponding author; *Email: mhossai5@kent.edu*

KOD JALUR / BARCODE
eISSN 2773-5958

Received: 31 May 2021
Accepted: 16 July 2021
Published: 02 August 2021
Volume -2, Issue-3
Cite This: *ICRRD Qual. Ind. Res. J.* 2021, 2(3), 109-119

ABSTRACT: The nanoparticles of ZnO (*n*-ZnO) have been synthesized by a sol-gel method and characterized by UV-visible and FTIR spectroscopy, scanning electron microscopy (SEM), energy dispersive X-Ray spectrometry (EDX) and powder X-ray diffractometry (XRD). Precursor of *n*-ZnO particles were prepared via a non-aqueous route, which was calcined at 500°C. These particles were then deposited on a glass substrate for adsorption and photodegradation of a typical textile dye, Remazol Red RR (RRR). Especially, the high surface to volume ratio of nanoparticles has appealed much attention to use these particles both as an adsorbent and a photocatalyst. A comparative study was carried out between *n*-ZnO and a commercially available ZnO (*c*-ZnO) to investigate the removal efficiency of RRR from its aqueous solution under different conditions. The removal efficiency has been optimized by varying several operating variables and the highest performance has been obtained with 0.115 g/slide of ZnO and 0.5×10^{-4} M aqueous solution of RRR under sunlight irradiation. It is important to note that the use of the films of ZnO in the presence of solar light makes it suitable for recycling and causes no secondary environmental pollution.

Keywords: *nanoparticles, ZnO film, heterogeneous photocatalysis, Remazol Red RR, adsorption, photodegradation*

INTRODUCTION

In the textile dying and knitting factories, significant amounts of synthetic dyes used during manufacturing and processing operations are lost to the effluent [1]. These dyes pose a serious threat to the ecosystem [2] because of their toxicity, inability for biodegradation, and carcinogenic nature, and cause serious harm to lives in the aquatic environment. However, international environmental regulations are becoming more demanding with increased public concern for these pollutants; thus, modern treatment approaches are required to eliminate or turn persistent dye organic chemicals into non-toxic compounds in water. For the treatment of dye-containing effluents, different research methods including biological [3, 4], physical [5-8], and chemical [9-11] methods have been carried out.

Dyes are typically mineralized by aerobic degradation and in some cases, carcinogenic compounds may be produced during this process. From this point of view, the biological method seems to be ineffective for the treatment of reactive dyes [12] and cost-intensive for some organic pollutants. The non-destructive physical methods such as adsorption, ion-exchange, reverse osmosis etc. only transfer the pollutants from one phase to another phase. Although some chemical methods, which are ozonation and chlorination, have led to successful mineralization of the pollutants, discharging of chlorinated compounds during the cleaning process causes severe problems for the ecosystem than the parent pollutants. On the other hand, the ozonation process requires in-situ ozone preparation and is not economically viable [13].

Recently, advanced oxidation processes (AOPs) have contrived to remove organic contaminants by following oxidative photodegradation with hydroxyl radicals (•OH). This radical is a powerful oxidizing agent that can non-selectively oxidize organic compounds into mineralized products such as carbon dioxide and water [14]. But this process relies on the in-situ preparation of hydroxyl radicals (•OH) which in turn relies on additional H_2O_2 in the presence of UV light. This involves significant capital costs. Nowadays, a higher extent of attention to metal oxide semiconductors has been observed owing to their potentiality of total mineralization of most of the organic contaminants into carbon dioxide, water and mineral acids [15-17]. This process of mineralization preserves marine life and makes the environment eco-friendly. For example, both ZnO and TiO_2 have the same band gap energies of 3.0-3.2 eV with corresponding radiation wavelengths of 410-380 nm [18]. Due to this large band gap energy, they can supply the most powerful oxidizing photo-generated electrons and holes. In the field of mineralization, not only this, but also their cost-effectiveness, great accessibility, and environmentally friendly approaches have attracted much attention to use them as photocatalysts. TiO_2 is used as the most efficient photocatalyst for some organic compounds [19-21]. Meanwhile, ZnO has also wide variety of applications for the photodegradation and complete mineralization of environmental pollutants [22-27].

The recent studies on the synthesis of nano-sized particles using a green chemistry approach have explored an excellent performance in the manifestation of eco-friendly, cost-effective, recyclable, and sustainable materials for applications in the future [28]. Nanomaterials display extraordinary photocatalyst behavior relative to those of bulk materials. This enhanced activity of nanomaterials mainly depends on their surface area, quantum confinement and correct facets of catalysts. A large number of quantized discrete electronic energy levels are created due to this quantum confinement, which increases the effective energy gap between the conduction and valence bands of a semiconductor [29]. As a result, the band edges shift to yield greater redox potentials. In this research, we have attempted to prepare nano-ZnO (*n*-ZnO) particles through a non-aqueous route. It is then used to test the suitability as a photocatalyst in the photodegradation of aqueous solution Remazol Red RR (RRR). The research findings for *n*-ZnO have been compared to those obtained from commercially available ZnO (*c*-ZnO). So far, many study groups have used *c*-ZnO as a photocatalyst [30,31]. However, an obvious goal for the researchers in this field is to improve the effectiveness of this oxide. On the other hand, in large-scale applications, the use of suspension of oxide particles involves the isolation and recycling of the fine catalyst from the processed wastewater prior to discharge into the aqueous environment. This process of wastewater treatment is time consuming and expensive. To avert this separation issue, *n*-ZnO films will be prepared on glass supports and their RRR dye removal efficiency from aqueous solution will be evaluated. The use of the films of ZnO in the presence solar light makes it suitable for recycling and causes no secondary environmental problems.

EXPERIMENTAL

The dye, RRR was obtained from DyStar, Germany and used here without further purification. All other chemicals such as zinc acetate dihydrate and oxalic acid dihydrate were purchased from Merck. De-ionized water was used for all the experiments.

A. Preparation of ZnO nanoparticles

About 11.0 g of zinc acetate dihydrate was dissolved in an open reactor containing 300 mL ethanol at 60°C. The salt was completely dissolved within 30 min. Similarly, 12.5 g of oxalic acid dihydrate was dissolved in another reactor with 200 mL ethanol at 50°C. Then a solution of oxalic acid was slowly added to the warm ethanolic solution of zinc acetate with continuous stirring. A white thick gel was formed which was then placed in an electric oven for drying at 80°C for 20 hours. The precursor of ZnO was then calcined at a temperature of 500°C for 2 hours to yield the *n*-ZnO particles. This process was repeated several times to prepare a sufficient quantity of *n*-ZnO particles for the complete study. UV-visible and IR spectroscopy, SEM, EDX, and XRD were used to characterize these prepared *n*-ZnO samples.

B. Preparation of glass supported ZnO film

About 1.0 g of prepared *n*-ZnO was taken in a beaker containing 15.0 mL de-ionized water to prepare an aqueous suspension which was sonicated for two hours for better dispersion. It was then placed on an antecedently weighted glass substrate (7.5 cm × 2.5 cm) by a simple immobilization method [32] and then kept for air dry and finally dried in an electric oven at 100°C for 4 hours. The amount of ZnO was then calculated by deducting the initial weight of the bare glass substrate from the film of ZnO at room temperature. Reproducibility of the films of the same mass was found to vary within ± 0.003 g. These films were kept in a desiccator and used for subsequent experiments.

C. Removal technique of RRR by *n*-ZnO and *c*-ZnO film

For the adsorption and photodegradation of RRR, *n*-ZnO and *c*-ZnO immobilized film was introduced into the aqueous solution of RRR (100 mL) in a reactor of inside diameter 8.0 cm, height 12.0 cm. After achieving the equilibrium time of adsorption, it was irradiated by light (UV and Solar light) with continuous stirring by a magnetic stirrer. The whole system was enclosed in a wooden box with a blackened entire surface when irradiation occurred by UV light. For solar light irradiation, the reactor was taken in an open place on a magnetic stirrer. For this latter experiment, the time was chosen from 11.00 AM to 2.00 PM, when the sunlight has the highest intensity in the months of April. For all experiments, aliquots of the sample were withdrawn at a definite interval of time and the absorption spectra were recorded using a UV-visible spectrophotometer (Shimadzu-1800) in the region of 200 to 800 nm.

RESULTS AND DISCUSSION

A. Characterization of n-ZnO

The UV-visible absorption spectrum of *n*-ZnO was taken in aqueous suspension and has been shown in Fig. 1 (left). A sharp peak is obtained at λ_{max} of 368 nm with corresponding band gap energy of 3.37 eV due to excitonic absorption from oxide nanoparticles. This hypsochromic shift shows the quantum confinement property of the nanoparticles. As the quantum confinement increases the band gap of the particles increases, as a result, absorption peak shifts to the lower wavelength region with decreasing particle size. It is also clear from the figure that quite a sharp absorption peak of *n*-ZnO indicates the monodispersed distribution of the nanoparticles [33,34].

IR absorption spectrum was taken by a Shimadzu FTIR-8300 spectrophotometer as pressed KBr-discs at room temperature. Fig. 1 (right) shows the FTIR spectrum of n-ZnO prepared at 500°C with characteristics band at 440 cm^{-1} that corresponds to the E_2 mode of hexagonal ZnO [35]. A series of peaks from 1630 to 820 cm^{-1} is due to the asymmetrical and symmetrical stretching of the zinc

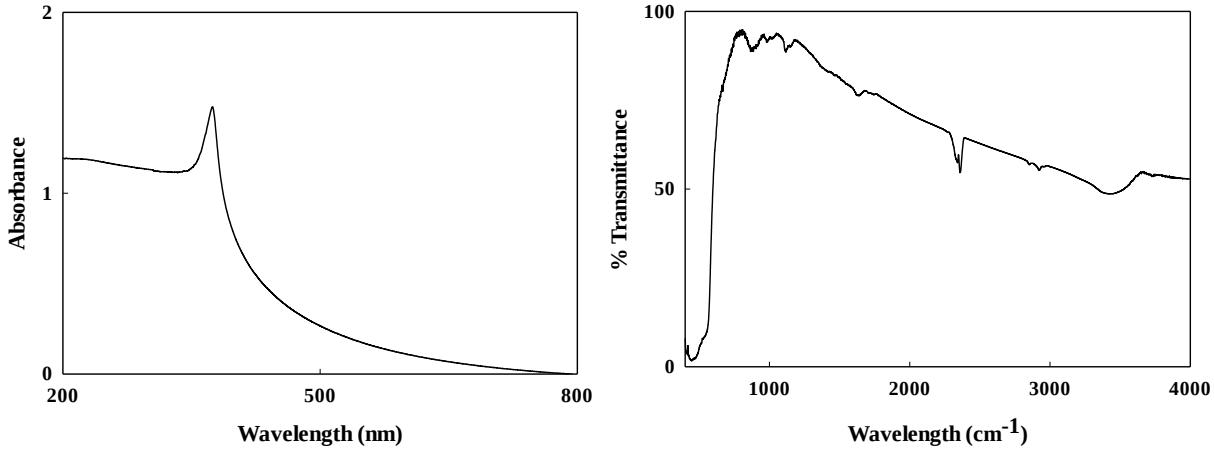

Fig. 1: Spectral analysis of prepared *n*-ZnO particles calcined at 500°C. UV-visible absorption spectrum (left) and FTIR absorption spectrum (right).

carboxylate which may be present in trace amount in the sample [36]. There is a broad band at around 3432 cm^{-1} due to -O-H stretching mode of the hydroxyl group. A commercially available ZnO powder sample was reported to show surface -OH groups around 3400 cm^{-1} [37]. Our results are consistent with those obtained by them. Moreover, it can be concluded that there is a lower surface coverage of the hydroxyl group on the prepared *n*-ZnO.

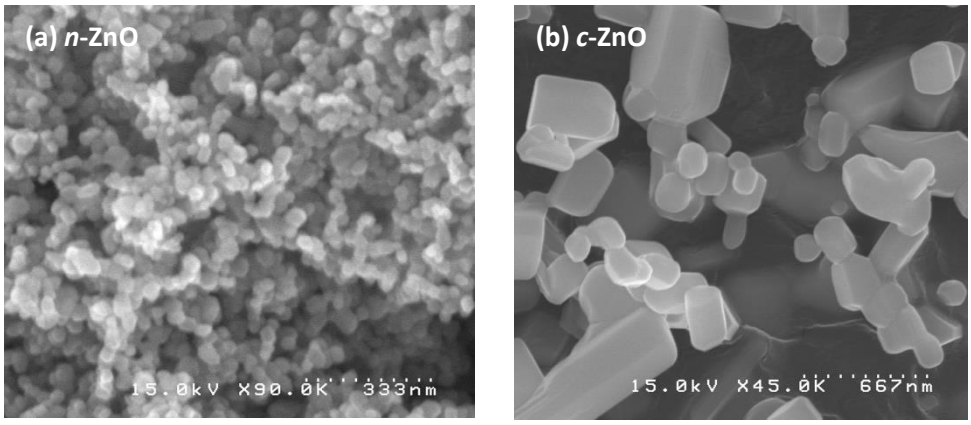

Fig. 2: Observation of surface morphology by SEM images. (a) for prepared *n*-ZnO particles calcined at 500°C and (b) for *c*-ZnO particles.

The surface morphology and crystalline structure of prepared *n*-ZnO particles were analyzed by SEM (Model: JSM-6490, JEOL). Fig. 2 represents the SEM images of prepared *n*-ZnO and *c*-ZnO particles at a suitable magnification. The image of *c*-ZnO is shown for comparison of the size and morphology of the particles. It affirms the formation of *n*-ZnO particles with a spherical structure. The average particle

size estimated from the image is 35 ± 5 nm, which is confirmed by XRD (discussed in latter section). The SEM image indicates a mono dispersed phase with a narrow size distribution. Random agglomeration of *n*-ZnO particles occurred due to their large surface to volume ratio and high surface energy [38]. On the other hand, *c*-ZnO presents expected crystalline particles having characteristic hexagonal wurtzite shape. The sizes of the particles show a wide range of distribution between 200 and 500 nm. This difference in the surface morphology is expected to affect both adsorption and photodegradation properties of these samples. The chemical composition of the prepared *n*-ZnO particles has been analyzed by EDX (Fig. 3). It urges that there is no trace amount of impurities present within the detection limit of the EDX other than Zn and O atoms.

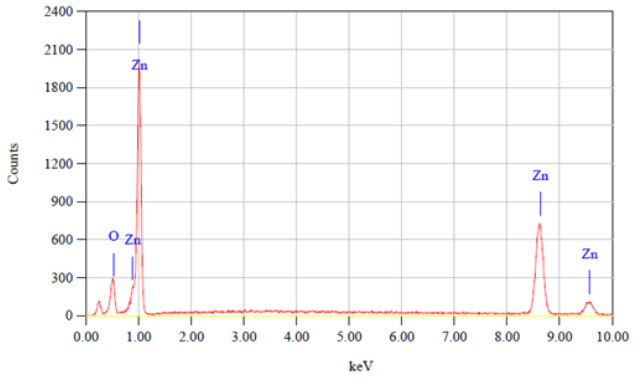

Fig. 3: EDX spectrum of *n*-ZnO calcined at 500°C.

The powder X-ray pattern was taken by Philips PW 1724 X-ray 700 generator using XDC-700 Guinier-Hägg focusing camera with strictly monochromatic Cu kα1 radiation (λ=1.540598 Å). The exposure time was 15 min at 40kv-30 mA and the diffraction pattern was recorded in an image plate. Image plates were scanned using an HD-CR 35 NDT scanner. A diffraction plot detects the intensity of diffracted X-rays as a function of 2θ. Fig. 4 illustrates the powder X-ray diffraction pattern for the prepared *n*-ZnO particles. From the diffraction data, all interlayer spacing (d-spacing) values were estimated from Bragg's equation. It was observed that the Bragg's peaks indexed at (100), (002), (101), (102), (110) and (103), (112) and (201) are analogous to the hexagonal wurtzite structure of ZnO (a = 3.249 Å, c = 5.192 Å) [35, 39]. These diffraction data are coincident with the JCPDS data of zincite (JCPDS 36-1451). It is also clear that the XRD pattern ascertains of good crystalline structures of prepared n-ZnO. No unnecessary diffraction peaks corresponding to impurity atoms are observed. The crystalline size of *n*-ZnO particles was calculated from the X-ray line broadening of the XRD peak corresponding to (0 0 2) reflection, using Debye-Scherrer formula [40]. The sizes of the particles agree with the results obtained from the SEM images.

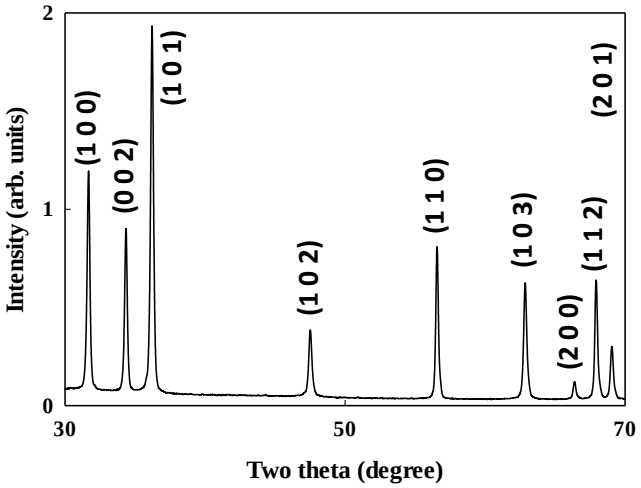

Fig. 4: XRD pattern of *n*-ZnO calcined at 500°C

B. Removal of RRR by glass supported *n*-ZnO film

The main purpose of preparing *n*-ZnO is to apply it as a photocatalyst and to determine its photocatalytic efficiency. For comparison, *c*-ZnO is also used under the same experimental conditions. RRR molecules were found to adsorb on both types of ZnO films. Therefore, the prepared glass supported ZnO films were kept for 40 minutes in an aqueous solution of RRR for achieving the same

film by irradiating under a light source. Fig. 5 shows the percent removal of the RRR from 1.0×10^{-4} M aqueous solution of dye with different amounts of *n*-ZnO catalyst dosages under UV light. It should be noted here that the sunlight was not used for optimization of amount of *n*-ZnO because of the difficulty related to the absence of constant light intensity at different times and days. The Fig. 5 shows that with an increase in the amount of catalyst of the film, the percent removal increases up to a catalyst dose of 0.115 g/slide. With a further increase in the catalyst dosage, the percent removal decreases. Initially, the percent removal increases due to the increase in the effective surface area of the *n*-ZnO particles. This conclusion is further supported by the percent removal vs. amount of ZnO with time variation data (Fig. 6) where an increasingly higher amount of dye removal is found with an increase in the amount of catalyst. Due to availability of more active surface sites, higher absorption of quanta by semiconductor induces direct band gap excitation and consequences in more electron-hole separation. These photogenerated holes oxidize the dye at the ZnO surface.[41] The percent removal becomes the maximum because the glass substrate covered by the catalyst becomes saturated with a definite amount of the ZnO. Therefore, a maximum removal of the dye including both adsorption and degradation was found at 0.115 g/slide. A further increase in the catalyst loading causes the percent removal to decrease gradually because the binding ability of film on the glass substrate decreases. Since the film thickness increases, some parts of the film are detached from the glass surface during photodegradation. This causes non-homogeneity of the surface of the films and decreases the dye removal efficiency.

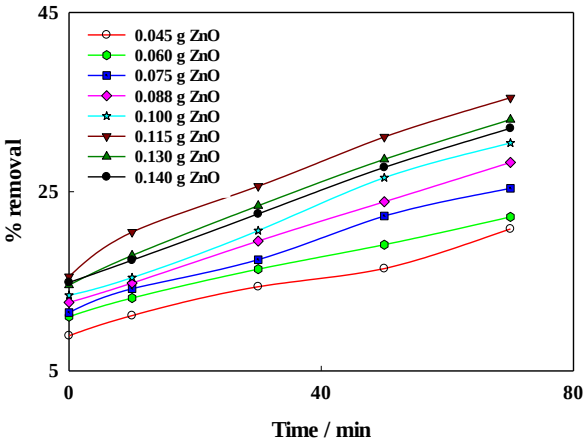

Fig. 5: Effect of catalyst dose on the removal of RRR by *n*-ZnO.

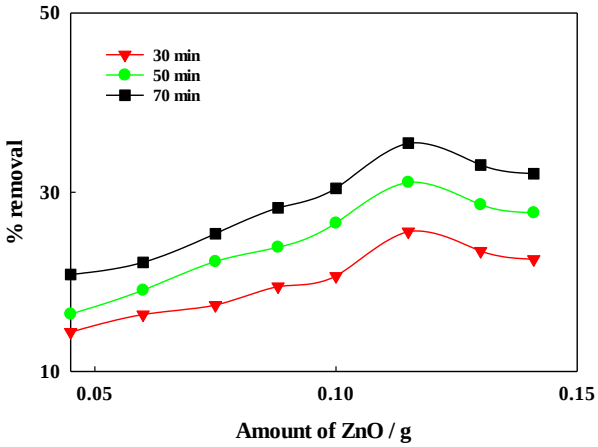

Fig. 6: Effect of time variation on the removal of RRR by *n*-ZnO.

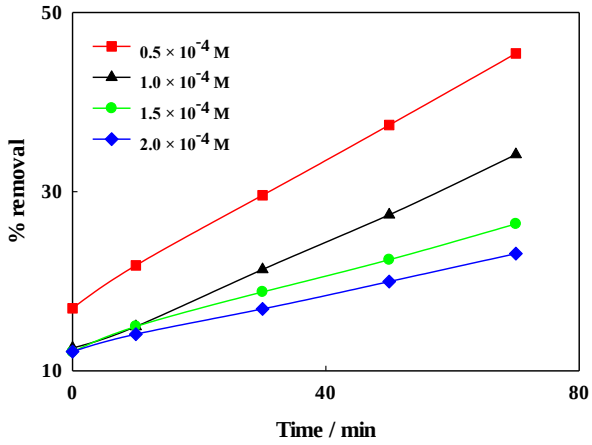

Fig. 7: Effect of dye concentration on the removal of RRR by *n*-ZnO.

To investigate the effect of initial RRR solution concentration on the removal of the dye, the initial concentration was varied between 0.5×10^{-4} M and 2.0×10^{-4} M using 0.115g/slide of ZnO and results are presented in Fig. 7. It has been

observed that the maximum percentage of removal is achieved by lower concentrations and vice-versa. This diminishing effect is due to two principal reasons: as the dye concentration increases equilibrium adsorption of dye on the catalyst surface active sites increases which reduce the adsorption rate of OH- ion on the same sites. As a result, lowering the rate of formation of •OH radical is the most powerful oxidizing agent for a high degradation efficiency. On the other hand, with an increase in the initial dye concentration, the path length of photons entering the solution decreases. This phenomenon of lowering the number of photon absorption by the catalyst particles may also reduce the degradation rate.[42]

Two light sources, artificial UV light and sunlight were employed for the purpose of photodegradation. Under all experimental conditions, the sunlight shows better dye removal efficiency compared to UV light (Fig. 8). These results are therefore important from the viewpoint of cost and environmental pollution. The energy of UV light is sufficient for the separation of electron-holes of the semiconducting ZnO. The solar light acts as a source of UV and all other energetic radiations. These combine radiations play an effective photogeneration of hot electrons and energetic holes on the surface of ZnO to oxidize the RRR. The photogenerated hole react with OH^- ion or water molecule to generate •OH radical and hot electron react with dissolve molecular oxygen to generate superoxide ($•O_2^-$) radical. Finally, both radicals participate to decompose the azo dye RRR and produce degraded inorganic molecules, CO_2, and water.[20]

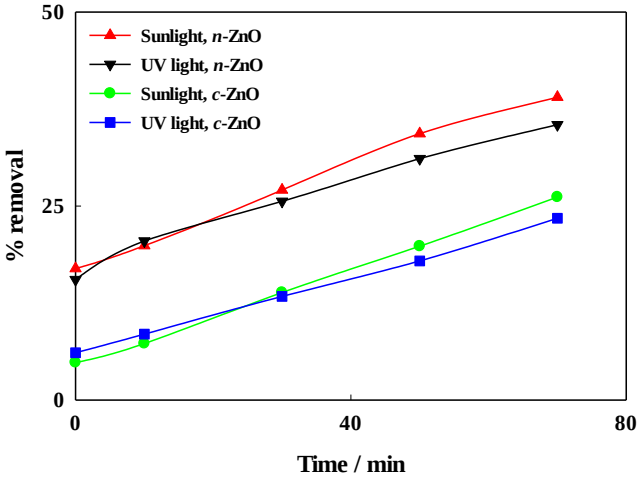

Fig. 8: Effect of different light sources on the removal of RRR by *n*-ZnO and *c*-ZnO

$ZnO + hv \rightarrow ZnO\ (h^+ + e^-)$ (1)

$h^+ + OH^-$ or $H_2O \rightarrow •OH + H^+$ (2)

$e^- + O_2 \rightarrow •O_2^-$ (3)

$•O_2^- + H^+ \rightarrow HO_2•$ (4)

RRR + (•OH, $•O_2^-$, and/or $HO_2•$) → Intermediate products. (5)

Intermediate products. + (•OH, $•O_2^-$, and/or $HO_2•$) → degraded products + $H^+ + CO_2 + H_2O$ (6)

Nanoparticles have a larger surface area and a strong quantum confinement that result in more adsorption,[5,8] photodegradation,[14] and capacitance measurement.[43] Fig. 8 shows the comparison of removal efficiency of RRR by both *n*-ZnO and *c*-ZnO at a fixed dye concentration of 1.0×10^{-4} M and with 0.115 g/slide of ZnO. It has been observed that the percent removal of the dye under 70 minutes sunlight irradiation in presence of *n*-ZnO is 37.3% whereas that of *c*-ZnO is only 23.4%. The average particle size of prepared *n*-ZnO is 35 ± 5 nm, whereas that of *c*-ZnO is in the range between 200 and 500 nm.

The percent removal of the dye comprising adsorption and photodegradation by *n*-ZnO film was monitored for a long time use of the film (Table 1). The result shows that the catalyst becomes less

effective with the time of photodegradation. This should be due to the instability of the film and the non-homogeneity of its surface.

Table-1: Effectiveness of *n*-ZnO film for long term use during the removal process under optimum conditions using sunlight.

Time / minutes	70	90	180	270
% removal	37.3	40.5	58.4	72.7

CONCLUSION

n-ZnO particles were successfully synthesized through a non-aqueous route with an average size of 35 ± 5 nm. The prepared nanoparticles were characterized by UV-visible spectroscopy, FTIR absorption spectroscopy, SEM, EDX, and XRD analysis. A glass supported *n*-ZnO film was developed for long term use of the catalyst and to overcome the time-consuming separation of suspended particles by centrifuging the treated wastewater prior to discharge. The experimental data showed that the *n*-ZnO particles are most effective than *c*-ZnO for the removal of RRR from aqueous solution. Moreover, the films are recyclable and the photodegradation can be carried out with the same films after the adsorption of dye. In addition, photodegradation under sunlight makes the removal technique eco-friendly and cost-effective. Although, complete removal of dye needs comparatively a longer time, further improvement of this methodology should lead to development of a cost-effective and eco-friendly technique for the treatment of industrial wastewater to maintain a green and sustainable environment.

ACKNOWLEDGEMENT: One of the authors (MMH) acknowledges the financial support from the Ministry of Education, Bangladesh.

CONFLICTS OF INTEREST

There are no conflicts to declare.

REFERENCES

[1] Z. Yang, H. Yang, Z. Jiang, T. Cai, H. Li, H. Li, A. Li, R. Cheng, Flocculation of both anionic and cationic dyes in aqueous solutions by the amphoteric grafting flocculant carboxymethyl chitosan-graft-polyacrylamide, Journal of Hazardous Materials, 254 (2013) 36-45.

[2] S. Khan, A. Malik, Toxicity evaluation of textile effluents and role of native soil bacterium in biodegradation of a textile dye, Environmental Science and Pollution Research, 25 (2018) 4446-4458.

[3] M. C. Cammarota, D. M. G. Freire, A review on hydrolytic enzymes in the treatment of wastewater with high oil and grease content, Bioresource Technology, 97 (2006) 2195-2210.

[4] G. Durai, M. Rajasimman. Biological Treatment of Tannery Wastewater-A Review, Journal of Environmental science and Technology, 4 (2011) 1-17.

[5] M. T. Yagub, T. K. Sen, S. Afroze, H. M. Ang, Dye and its removal from aqueous solution by adsorption: A review, Advances in Colloid and Interface Science, 209 (2014) 172-184.

[6] M. J. Miah, M. N. Kayes, M. Obaidullah, M. M. Hossain, Preparation of ZnO, Its Characterization and Effectiveness in Wastewater Treatment, Research Journal of Chemical and Environmental Sciences, 4 (2016) 50-57.

[7] Y. Safa, H. N. Bhatti, Biosorption of Direct Red-31 and Direct Orange-26 dyes by rice husk: Application of factorial design analysis, Chemical Engineering Research and Design, 89 (2011) 2566-

2574.
[8] H. A. Aziz, S. Alias, M. N. Adlan, Faridah, A. H. Asaari, M. S. Zahari, Colour removal from landfill leachate by coagulation and flocculation processes, Bioresource Technology, 98 (2007) 218-220.
[9] E. Rahmani, M. Rahmani, H. R. Silab, TiO2:SiO2 thin film coated annular photoreactor for degradation of oily contamination from wastewater, Journal of Water Process Engineering, 37 (2020) 101374.
[10] S. Mohanty, S. Moulick, S. K. Maji, Adsorption/photodegradation of crystal violet (basic dye) from aqueous solution by hydrothermally synthesized titanate nanotube (TNT), Journal of Water Process Engineering, 37 (2020) 101428.
[11] I. Arslan-Alaton, A. Kornmueller, M. R. Jekel, Contribution of free radicals to ozonation of spent reactive dyebaths bearing aminofluorotriazine dyes, Coloration Technology, 118 (2002) 185-190.
[12] S. Ledakowicz, M. Solecka, R. Zylla, Biodegradation, decolorization and detoxification of textile wastewater enhanced by advanced oxidation processes, Journal of Biotechnology, 89 (2001) 175-184.
[13] T. Robinson, G. McMullan, R. Marchant, P. Nigam, Remediation of dyes in textile effluent: a critical review on current treatment technologies with a proposed alternative, Bioresource Technology, 77 (2001) 247-255.
[14] I. K. Konstantinou, T. A. Albanis, TiO2-assisted photocatalytic degradation of azo dyes in aqueous solution: kinetic and mechanistic investigations: A review, Applied Catalysis B: Environmental, 49 (2004) 1-14.
[15] O. M. Shibin, S. Yesodharan, E. P. Yesodharan, Sunlight induced photocatalytic degradation of herbicide diquat in water in presence of ZnO, Journal of Environmental Chemical Engineering, 3 (2015) 1107-1116.
[16] J. Nishio, M. Tokumura, H. T. Znad, Y. Kawase, Photocatalytic decolorization of azo-dye with zinc oxide powder in an external UV light irradiation slurry photoreactor, Journal of Hazardous Materials, 138 (2006) 106-115.
[17] S. Rabindranathan, S. Devipriya, S. Yesodharan, Photocatalytic degradation of phosphamidon on semiconductor oxides, Journal of Hazardous Materials, 102 (2003) 217-229.
[18] S. George, S. Pokhrel, Z. Ji, B. L. Henderson, T. Xia, L. Li, J. I. Zink, A. E. Nel, L. Mädler, Role of Fe Doping in Tuning the Band Gap of TiO2 for the Photo-Oxidation-Induced Cytotoxicity Paradigm, Journal of the American Chemical Society, 133 (2011) 11270-11278.
[19] V. K. Gupta, R. Jain, A. Mittal, T. A. Saleh, A. Nayak, S. Agarwal, S. Sikarwar, Photo-catalytic degradation of toxic dye amaranth on TiO2/UV in aqueous suspensions, Materials Science and Engineering: C, 32(2012) 12-17.
[20] U. Afrin, M. R. Mian, B. K. Breedlove, M. M. Hossain, Enhanced Photocatalytic Activity of an Acid-modified TiO2 Surface for Degradation of the Azo Dye Remazol Red. Chemistry Select. 2 (2017) 10371-10374.
[21] S. Kaur, V. Singh, TiO2 mediated photocatalytic degradation studies of Reactive Red 198 by UV irradiation,Journal of Hazardous Materials, 141 (2007) 230-236.
[22] M. B. Akin, M. Oner, Photodegradation of methylene blue with sphere-like ZnO particles prepared via aqueous solution, Ceramics International, 39 (2013) 9759-9762.
[23] M. J. Height, S. E. Pratsinis, O. Mekasuwandumrong, P. Praserthdam, Ag-ZnO catalysts for UV-photodegradation of methylene blue, Applied Catalysis B: Environmental, 63 (2006) 305-312.
[24] M. M. Hossain, M. A. Hossain, M. N. Kayes, D. Halder. ZnO Mediated Photodegradation of Aqueous Solutions of Crystal Violet and Ponceau S by Visible Light. Journal of Engineering Science, 5 (2014) 69-74.

[25] X. Chen, Z. Wu, D. Liu, Z. Gao, Preparation of ZnO Photocatalyst for the Efficient and Rapid Photocatalytic Degradation of Azo Dyes, Nanoscale Research Letters, 12 (2017) 143.
[26] T. K. Tan, P. S. Khiew, W. S. Chiu, S. Radiman, R. Abd-Shukor, N. M. Huang, H.N. Lim, The Photodegradation of Organic Compounds by ZnO Nanopowder,Advanced Materials Research, 895 (2014) 547-557.
[27] M. T. Thein, S-Y.Pung, L. S. Chuah, Y-F. Pung, Photodegradation behavior of ZnO nanorods on various types of organic dyes, Advances in Materials and Processing Technologies, 4 (2018) 272-280.
[28] N. Narayan, A. Meiyazhagan, R. Vajtai, Metal Nanoparticles as Green Catalysts, Materials, 12 (2019) 3602.
[29] M. Stylidi, D. I. Kondarides, X. E. Verykios, Pathways of solar light-induced photocatalytic degradation of azo dyes in aqueous TiO2 suspensions, Applied Catalysis B: Environmental, 40 (2003) 271-286.
[30] M. Saquib, M. Muneer, Semiconductor mediated photocatalysed degradation of an anthraquinone dye, Remazol Brilliant Blue R under sunlight and artificial light source, Dyes and Pigments, 53 (2002) 237-249.
[31] N. K. Singh , S. Saha, A. Pal, Solar light-induced photocatalytic degradation of methyl red in an aqueous suspension of commercial ZnO: a green approach, Desalination and Water Treatment, 53 (2015) 501-514.
[32] M. N. Kayes, M. J. Miah, M. Obaidullah, M. A. Hossain, M. M. Hossain, Immobilization of ZnO Suspension on Glass Substrate to Remove Filtration During the Removal of Remazol Red R from Aqueous Solution, Journal of Advances in Chemistry, 12 (2016) 4127-4133.
[33] L. S. Panchakarla, A. Govindaraj, C. N. R. Rao, Formation of ZnO Nanoparticles by the Reaction of Zinc Metal with Aliphatic Alcohols, Journal of Cluster Science, 18 (2007) 660-670.
[34] P. Jamdagni, P. Khatri, J. S.Rana, Green synthesis of zinc oxide nanoparticles using flower extract of Nyctanthes arbor-tristis and their antifungal activity, Journal of King Saud University - Science, 30 (2018) 168-175.
[35] A. Kaschner, U. Haboeck, M. Strassburg, M. Strassburg, G. Kaczmarczyk, A. Hoffmann, C. Thomsen, A. Zeuner, H. R. Alves, D. M. Hofmann, B. K. Meyer, Nitrogen-related local vibrational modes in ZnO:N, Applied Physics Letters, 80 (2002) 1909-1911.
[36] G. Xiong, U. Pal, J. G. Serrano, K. B. Ucer, R. T. Williams, Photoluminescence and FTIR study of ZnO nanoparticles: the impurity and defect perspective, Physica Status Solidi (C), 3 (2006) 3577–3581.
[37] C. Hariharan, Photocatalytic degradation of organic contaminants in water by ZnO nanoparticles: Revisited, Applied Catalysis A: General, 304 (2006) 55-61.
[38] A. Muthuvinayagama, B. Thomasb, P. D. Christyc, R. J. Vijaya, T. M. Davidd, P. Sagayaraja, Investigation on the Sol-Gel Synthesis, Structural, Optical and Gas sensing Properties of Zinc Oxide Nanoparticles, Archives of Applied Science Research, 3 (2011) 256-264.
[39] C. Chen, B. Yu, P. Liu, J-Y. Liu, L. Wang, Investigation of nano-sized ZnO particles fabricated by various synthesis routes, Journal of Ceramic Processing Research, 12 (2011) 420-425.
[40] N. P. M. Aneesh, K. A. Vanaja, M. K. Jayaraj, Synthesis of ZnO nanoparticles by hydrothermal method, Proc. SPIE 6639, Nanophotonic Materials, IV (2007) 66390J.
[41] W. Z. Tang, Z. Zhang, H. An, M. O. Quintana, D. F. Torres, TiO2/UV Photodegradation of Azo Dyes in Aqueous Solutions, Environmental Technology, 18 (1997) 1-12.
[42] M. H. Abdellah, S. A. Nosier, A. H. El-Shazly, A. A. Mubarak, Photocatalytic decolorization of methylene blue using TiO2/UV system enhanced by air sparging, Alexandria Engineering Journal, 57 (2018) 3727-3735.

[43] A. C. Dassanayake, N. P. Wickramaratne, M. A. Hossain, V. S. Perera, J. Jeskey, S. D. Huang, H. Shen and M. Jaroniec, Prussian Blue-Assisted One-Pot Synthesis of Nitrogen-Doped Mesoporous Graphitic Carbon Spheres with Embedded Iron Oxide Nanoparticles. J. Mater. Chem. A, 7 (2019) 22092-22102.